40th Fluid Dynamics Conference and Exhibit, 28 Jun - 1 Jul 2010, Chicago, Illinois

Transition of hypersonic flow past flat plate with roughness elements

Prahladh S Iyer* , Suman Muppidi† and Krishnan Mahesh‡
University of Minnesota, Minneapolis, Minnesota, 55455, USA

Roughness elements in high speed flows can cause laminar-turbulent transition leading to higher heating rates and drag. Transition of flow past a hemispherical bump placed on a flat plate is explored in this paper for three Mach numbers [3.37, 5.26, 8.23] using direct numerical simulation on unstructured grids. The simulation parameters are chosen to match the experiments carried out by Danehy *et al*.[1] The wall is at a constant temperature of 300K. For flow conditions corresponding to Ma=3.37 and 5.26, unsteady flow structures were observed while for Ma=8.23, the flow remained laminar downstream of the trip. The location of transition was closer to the trip for the lowest Mach number. Qualitative comparison between the computation and experiment show good agreement. Based on the computed skin friction coefficient values, Ma=3.37 appeared to become turbulent in nature, Ma=5.26 was transitional and Ma=8.23 was laminar. Quantitative comparisons of flow profiles downstream of the trip were made with theoretical turbulent profiles to confirm transition to turbulence. The effect of distributed roughness on transition was also studied at Ma=2.9. A laminar boundary layer at Ma=2.9 was observed to transition to a turbulent boundary layer that shows good quantitative agreement with experimental data. The free-stream Mach number and roughness amplitude were seen to strongly influence whether or not the flow transitions. A local Reynolds number based on bump/roughness amplitude is seen to correlate the tendency to transition for both single bump and distributed roughness cases.

Nomenclature

ρ	Density	u	Velocity
p	Pressure	T	Temperature
E_T	Total Energy	σ_{ij}	Viscous shear stress
Q_i	Heat flux	Ma	Free stream Mach number
Re	Free stream unit Reynolds number	Re_d, Re_k	$\rho_\infty d u_\infty/\mu_\infty$, $\rho_\infty k u_\infty/\mu_\infty$
$Re_{d,wall}$	$\rho_{wall} d u_\infty/\mu_{wall}$	u_c	Van Driest transformed velocity
C_f	Skin friction coefficient		
Subscript			
CV	control volume	k	roughness length scale
d	diameter of hemispherical bump	∞	free-stream

*Graduate student, Dept. of Aerospace Engineering and Mechanics, University of Minnesota, Mn 55455, Student member.
†Research Associate, Dept. of Aerospace Engineering and Mechanics, University of Minnesota, MN 55455, Member.
‡Professor, Dept. of Aerospace Engineering and Mechanics, University of Minnesota, MN 55455, Associate Fellow.

I. Introduction

Studying laminar-turbulent transition in supersonic and hypersonic boundary layer flows is essential for the design of space vehicles and the prediction and control of heat transfer during re-entry. In the STS-114 Space Shuttle Return-to-Flight(RTF) mission, a space walk had to be performed to remove a protruding piece of gap filler material to avoid the effects of laminar-turbulent transition.[2] Schneider[3] gives a comprehensive review of the effects of roughness on hypersonic boundary layer transition. Some of the suggested mechanisms include the concave-wall Gortler instability,[4] the first- and second-mode streamwise-instability described by Mack,[5] the 3-D crossflow instability,[6] and transient growth.[7] Also, empirical based models like the Re_θ/M criterion are often used to predict the onset of transition.[8]

While the effect of roughness on transition for incompressible flows has been fairly well documented in the literature e.g. Tani,[9] Dryden,[10] Klebanoff,[11] Acarlar and Smith,[12] reliable experimental and computational data is limited for supersonic and hypersonic flows. Acarlar and Smith[12] have shown that for incompressible flow past a hemispherical roughness element, the presence of strong inflexional velocity profiles downstream of the hairpin-vortex generation region evolve into turbulent boundary layer velocity profiles with increasing downstream distance. Acarlar and Smith show that the presence of a standing horseshoe-shaped vortex makes the flow more unstable by comparing the flow past a hemisphere and a half teardrop. Tani[9] studied the effect of Re_k and showed that increasing Re_k beyond a critical value moves the transition location closer to the roughness. Tani suggests that the deformation of the velocity field due to the streamwise vortices (observed even at sub-critical Re_k) shed on the sides of the hemisphere is likely to account for the critical behavior of transition. Hall[13] examined transition by spheres suspended at various heights above a flat plate within a developing boundary layer. Comparing the wavelengths of the shed vortices with the minimum unstable wavelengths of two-dimensional disturbances for a similar undisturbed laminar boundary layer, Hall concluded that the mechanism by which laminar to turbulent transition occurred was dependent upon the stability characteristics of the element wake rather than the stability characteristics of the boundary layer.

Danehy *et al*[1,2] studied hemispherical, triangular and rectangular boundary-layer trips placed in supersonic and hypersonic flow over a flat plate. They observed that at higher Mach numbers, the impact of the roughness element was lower and the flow remained steady. At lower Mach numbers, unsteady structures were observed downstream of the roughness element indicating that the flow was either transitional or turbulent. Also, the onset of transition occurred closer to the roughness element for lower Mach numbers. Chang and Choudhari[14] numerically studied the effect of large roughness elements using a compressible Navier-Stokes code based on the space-time conservation element, solution element (CESE) method. They studied flow past rectangular and cylindrical elements at Mach numbers of 4.1 and 6.5. They concluded that for these Mach numbers, no self-sustained vortex generation was present. They also performed a 2D parametric study and found that at subcritical Reynolds numbers of the boundary layers, absolute instability resulting in vortex shedding downstream was likely to weaken at supersonic free-stream conditions and conjectured that convective instability might be the dominant instability mechanism for supersonic boundary layers. Redford *et al*[15] proposed a correlation for predicting transition induced by a three dimensional roughness element at high-speeds.

This paper uses DNS to study transition induced by (I) an isolated hemispherical bump on Mach 3.37, 5.26 and 8.23 boundary layer and (II) distributed roughness on a Mach 2.9 boundary layer. The single bump simulations are performed at conditions that match those in Danehy *et al.*[1] for the flow past an isolated hemispherical roughness. We use a novel algorithm developed by Park & Mahesh[16] to simulate compressible flows on unstructured grids. It employs a modified least–squares approach to reconstruct the fluxes at cell faces (that makes the convective flux computation more accurate), and a scheme to split the viscous stress tensor into the compressible and the incompressible parts (that makes the viscous flux computation accurate). A characteristic filter based shock capturing scheme provides stable solutions in the presence of discontinuities.

The algorithm used is described in Section II followed by a description of the simulation parameters and

computational mesh used in the simulation. Section IV compares the results to experiment and discusses the flow features downstream of the roughness. Results for skin friction, Van Driest transformed velocity profiles at different stations, and instantaneous contours of density and velocity are discussed. Section IV.D presents results from the distributed roughness simulations and Section IV.E discusses local Reynolds number as a parameter that is well correlated with the onset of transition.

II. Governing Equations and Numerical Details

The algorithm solves the compressible flow equations on unstructured grids. The governing equations are

$$\begin{aligned} \frac{\partial \rho}{\partial t} &= -\frac{\partial}{\partial x_k}\left(\rho u_k\right), \\ \frac{\partial \rho u_i}{\partial t} &= -\frac{\partial}{\partial x_k}\left(\rho u_i u_k + p\delta_{ik} - \sigma_{ik}\right), \\ \frac{\partial E_T}{\partial t} &= -\frac{\partial}{\partial x_k}\left\{\left(E_T + p\right)u_k - \sigma_{ik}u_i - Q_k\right\}, \end{aligned} \tag{1}$$

where ρ, u_i, p and E_T are density, velocity, pressure and total energy, respectively. The viscous stress σ_{ij} and heat flux Q_i are given by

$$\sigma_{ij} = \frac{\mu}{Re}\left(\frac{\partial u_i}{\partial x_j} + \frac{\partial u_j}{\partial x_i} - \frac{2}{3}\frac{\partial u_k}{\partial x_k}\delta_{ij}\right), \tag{2}$$

$$Q_i = \frac{\mu}{(\gamma-1)M_\infty^2 RePr}\frac{\partial T}{\partial x_i} \tag{3}$$

after standard non-dimensionalization, where Re, M_∞ and Pr denote the Reynolds, Mach and Prandtl numbers.

The governing equations are discretized using a cell–centered finite volume scheme. Upon integration over the control volume, and application of the Gauss theorem, and some rearrangement, the governing equations may be written as

$$\begin{aligned} \frac{\partial \rho_{\rm cv}}{\partial t} &= -\frac{1}{V_{\rm cv}}\sum_{\rm faces}\rho_f v_N A_f, \\ \frac{\partial\left(\rho u_i\right)_{\rm cv}}{\partial t} &= -\frac{1}{V_{\rm cv}}\sum_{\rm faces}\left[\left(\rho u_i\right)_f v_N + p_f n_i - \sigma_{ik,f}n_k\right]A_f, \\ \frac{\partial\left(E_T\right)_{\rm cv}}{\partial t} &= -\frac{1}{V_{\rm cv}}\sum_{\rm faces}\left[\left(E_T + p\right)_f v_N - \sigma_{ik,f}u_{i,f}n_k - Q_{k,f}n_k\right]A_f, \end{aligned} \tag{4}$$

where $V_{\rm cv}$ is the volume of CV, A_f is the area of the face, n_i is the outward normal vector at surface, and v_N is the face-normal velocity. $\mathbf{q}_{\rm cv} = \left(\int_{\rm cv}\mathbf{q}dV\right)/V_{\rm cv}$ is the volume average within the cell, where $\mathbf{q} = (\rho, \rho u_i, E_T)$ are the conservative variables. Here, the subscript f denotes the interpolation at each face of the control volume. The simulations employ a Modified least–square method (Park and Mahesh[16]) for face reconstruction, which is more accurate than a simple symmetric reconstruction, and more stable than a least–square reconstruction. The algorithm uses a novel shock–capturing scheme that localizes numerical dissipation to the vicinity of flow discontinuities, thereby minimizing unnecessary dissipation. The solution is advanced in time using a second–order explicit Adams–Bashforth scheme, as

$$q_j^{n+1} = q_j^n + \frac{\Delta t}{2}\left[3{\rm rhs}_j(\mathbf{q}^n) - {\rm rhs}_j(\mathbf{q}^{n-1})\right], \tag{5}$$

where rhs_j denotes j th component of r.h.s. of Eq. (4), and superscript n denotes n th time step. The algorithm has been validated for a variety of simple problems, as presented in Park and Mahesh.[16]

III. Problem description

The parameters used in the single bump simulation match those in the experiment carried out by Danehy *et al*[1] in the 31-Inch Mach 10 Air Tunnel at NASA Langley Research Center. In the experiment, a 20° full-angle wedge was placed in the path of a Mach 10 flow at five different angles of attack with respect to the oncoming flow chosen at equal intervals between 5° and 25°. Two different stagnation pressures were used in the experiment corresponding to unit Reynolds numbers of 3.3 million/m and 6.1 million/m. We simulate the flow past the top surface of the wedge which is equivalent to flow past a flat plate for unit Reynolds number corresponding to 6.1 million/m. We simulate the lowest, intermediate and highest Mach number corresponding to wedge angles of 25°, 15° and 5°. The post-shock conditions of the leading edge shock formed at the wedge tip serve as the free-stream conditions for different wedge angles. The free-stream conditions were calculated using theoretical oblique shock relations and also verified with the experimentally measured conditions. The resulting free-stream conditions are shown in Table 1. The Reynolds number is calculated based on the diameter of the hemisphere which is 4 mm. All length scales are non-dimensionalized with respect to the diameter of the hemisphere and the non-dimensional free-stream velocity and density is taken as unity.

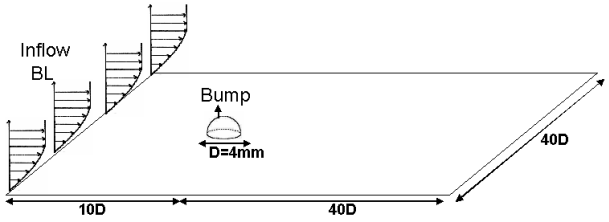

Figure 1. Schematic of the flow past an isolated hemispherical roughness element

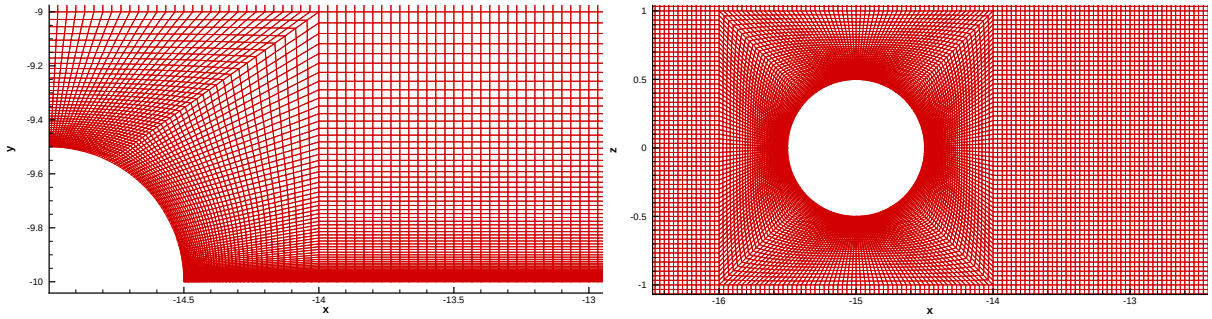

Figure 2. Plots showing the grid used in the simulation in the symmetry plane(left) and wall normal plane very close to the flat plate(right).

In the experiment, the hemisphere was placed at a non-dimensional distance of 18.85 units downstream of the leading edge of the wedge which was 32 units wide. Further details can be found in Danehy*et al.*[1] The computational domain extends from -25 to 25 units in the streamwise direction, -20 to 20 units in the spanwise direction and -10 to 10 units in the wall normal direction. The hemisphere is located at x=-15 (10 units downstream of the inflow). A compressible similarity solution at conditions corresponding to a streamwise distance of 8.85 units is prescribed at the inflow. It is assumed that the influence of the roughness element is negligible at distances beyond 10 diameters upstream of the hemispherical bump. As discussed

later, the C_f at distances beyond 5 diameters upstream of the bump matches well with the laminar value, confirming the validity of our assumption. A sponge layer[17] is used at the inflow between x=-25 and -22 to absorb any upstream traveling disturbances that might be created when the solution changes from a similarity solution to a full 3D Navier-Stokes equation. An isothermal wall condition with T_{wall}=300K is prescribed for all the three cases being simulated. An extrapolation boundary condition where the solution is extrapolated from the interior points is prescribed for the top, side and outflow walls.

Ma	Re_d	Temperature (free-stream)
3.37	18241	340 K
5.26	28379	162.9 K
8.23	33662	73K

Table 1. Parameters used in the simulation

The grid is composed of 40 million elements with a maximum of 860 grid points in the streamwise direction, 500 grid points in the spanwise direction and 182 grid points in the wall normal direction. A close up of the grid around the bump is shown in Fig. 2. The grid is composed of hexahedral elements. More than 70 grid points are placed within the boundary layer downstream of the bump.

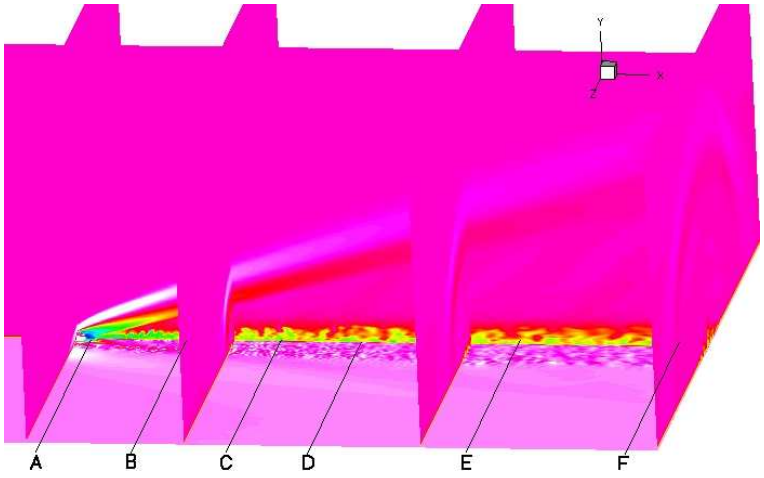

Figure 3. 3d contours of instantaneous density for Ma=3.37.

To illustrate the different flow features associated with the problem, Fig. 3 shows instantaneous contours of density for Ma=3.37. Note the shock produced by the roughness element. The angle of the shock is maximum for the lowest Mach number as observed in later sections. The figure shows the shock exiting the domain for the lowest Mach number simulation, indicating that the height of the domain is adequate for all three cases. Behind the bump, note the presence of unsteady structures which appear to breakdown as we move downstream, suggesting transitional/turbulent flow for this Mach number. Fig. 3 also shows various streamwise stations marked A to F at which quantitative comparison and analysis of the velocity profile will be performed in Section IV. Stations A through F are located at distances of 0.5, 4, 10, 15, 25 and 35 bump diameters respectively from the center of the bump.

IV. Results

The flow past a hemispherical bump is simulated for Mach numbers 3.37, 5.26 and 8.23 with other conditions as specified in Table 1. The simulation parameters match those of the experiment by Danehy *et al*[1] and results from the computations are compared to the available data from the experiments. Note that only the roughness shape and height, and isothermal wall temperature are same for the three cases considered. Factors such as boundary layer thickness, Reynolds number and free-stream temperature which influence transition, all change between the three cases.

IV.A. Qualitative comparison to experiment

Figure 4 compares instantaneous contours of vorticity magnitude on the symmetry plane to NO-PLIF images obtained from experiment. Good qualitative agreement is observed. Unsteady structures appear behind the bump for the lower Mach number cases while the flow appears to be steady for the highest Mach number. The unsteady structures form closer to the bump for Ma=3.37 as compared to Ma=5.26. Smaller scale structures form as we move downstream for the lower Mach number cases, suggesting that the flow is transitional/turbulent. The boundary layer thickness of the flow upstream is least for Ma=3.37 and is highest for Ma=8.23. If the boundary layer thickness just upstream of the roughness element is taken as the relevant length scale of the problem, a lower boundary layer thickness means that the flow sees a larger roughness element. It is known in incompressible flows that larger roughness elements move the transition location forward towards the roughness and the observations from Fig. 4 are consistent with the incompressible trends. Quantitative data from the PLIF experiment is unavailable for comparison.

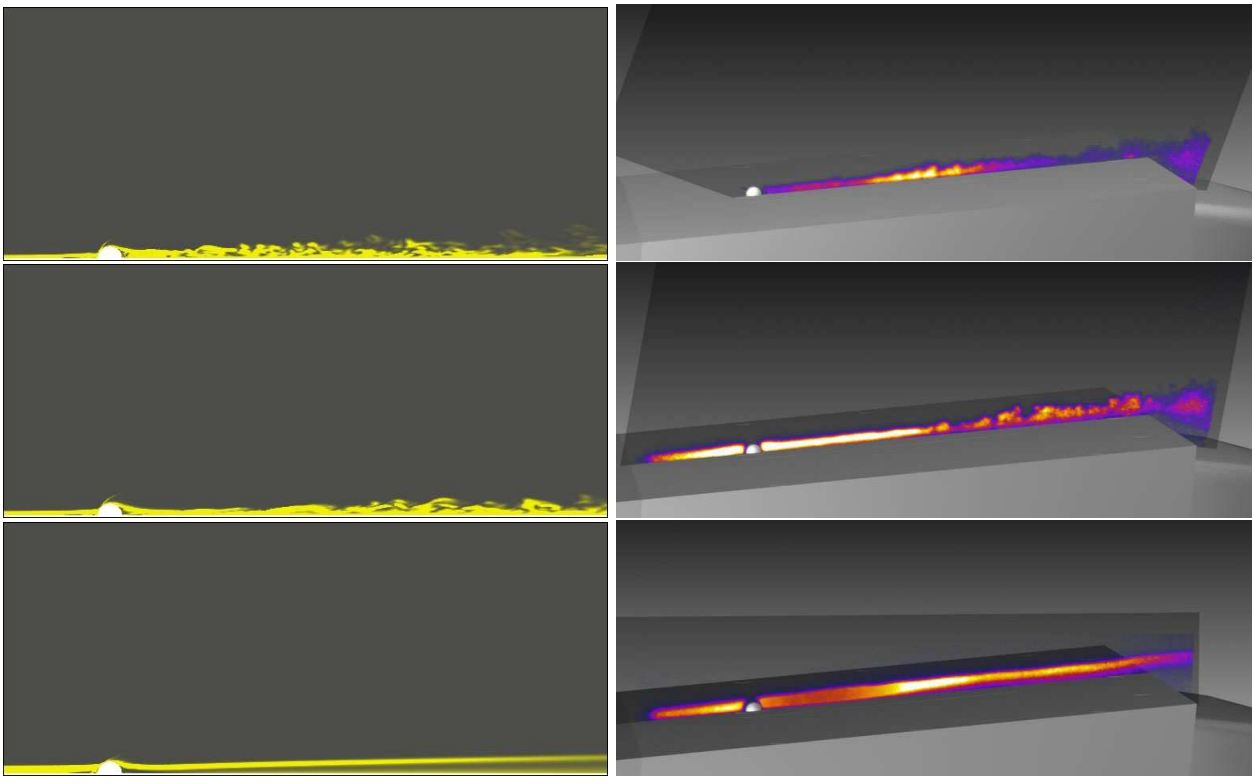

Figure 4. Vorticity magnitude contours from DNS(left) and NO-PLIF images from Danehy *et al*(right) for Ma=3.37(top), Ma=5.26(center) and Ma=8.23(bottom).

IV.B. Nature of flow

To assess the effect of the hemispherical roughness element on the incoming laminar boundary layer, we study the variation of skin friction coefficient and compare the Van Driest transformed velocity at different stations in the symmetry plane to expected turbulent profiles. The distortion of the mean velocity field by the roughness element could make the laminar boundary layer turn turbulent, become transitional or remain steady and laminar downstream of the roughness. Fig. 5 shows the streamwise variation of the skin friction coefficient(C_f) in the symmetry plane for all three cases. Also shown are the theoretical skin friction coefficients for laminar and turbulent boundary layers. The laminar skin friction coefficient is computed from the compressible similarity solution assuming there is no roughness element present. The skin friction coefficient for a turbulent boundary layer is computed from Schlichting[18] where the C_f is obtained from an experimental curve of the ratio of compressible to incompressible C_f at different Mach numbers with heat transfer. From Fig. 5, it can be observed that for all three Mach numbers, the agreement between the C_f obtained from DNS and the theoretical laminar value is excellent upstream of the bump. The effect of the recirculation and separation bubble causing the C_f to go negative can be observed for all three cases. The low pressure region created downstream of the separation bubble causes high momentum fluid away from the wall to move towards the wall thus causing the C_f to increase. The effect of the separation bubble is most prominent for the lowest Mach number case as observed by the sharp increase in the C_f value and least prominent for Ma=8.23 where the C_f remains close to the theoretical laminar value. We observe that C_f rises to the theoretical turbulent value close to 10 diameters downstream of the bump for Ma=3.37 and oscillates around the theoretical turbulent value further downstream. This indicates that the Ma=3.37 flow becomes turbulent as it moves downstream of the bump. For Ma=5.26, we see that the C_f is slightly less than the laminar value until about 15 diameters downstream indicating that the flow is probably laminar in this region. Beyond 15 diameters, the C_f rises close to the turbulent value and oscillates about a value that lies between the laminar and turbulent C_f values indicating that the flow is transitional in nature. The flow remains transitional until the end of the domain (35 diameters downstream of the bump). For Ma=8.23, the C_f downstream of the bump remains very close to the laminar value. Downstream of the separation bubble, the C_f gradually rises to reach the theoretical laminar value close to the outflow. The quantitative trends showing the nature of the flow and location downstream at which unsteady flow structures appear observed in Fig. 5 is consistent with the qualitative trends observed in Fig. 4.

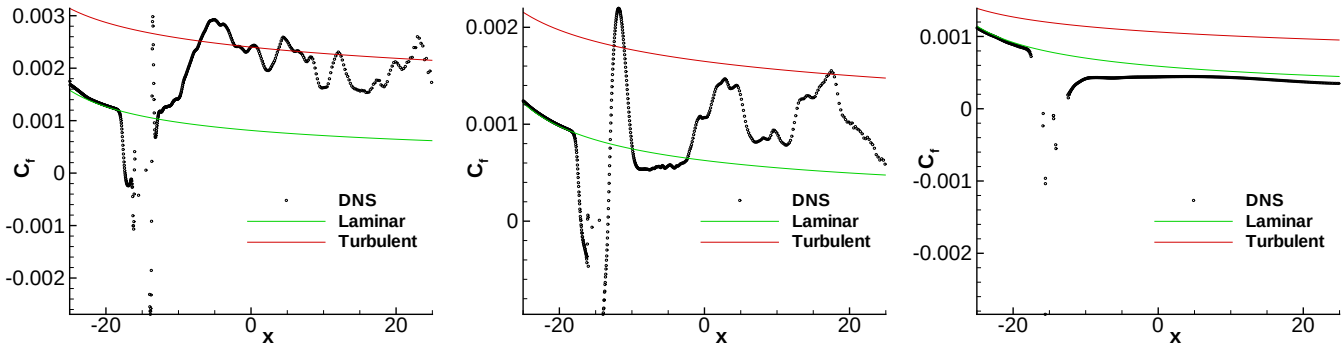

Figure 5. Skin friction coefficient variation with streamwise distance in symmetry plane for Ma=3.37(left), Ma=5.26(center) and Ma=8.23(right).

Figure 6 shows the Van Driest transformed velocities for all three cases and compares it to expected behavior. The stations C, D, E and F are located at downstream distances as specified in Section III. For all three cases, the near wall behavior agrees with the expected profile until $y^+ = 3.0$ and then begins to deviate. For Ma=3.37, only station C obeys the log layer profile for the turbulent boundary layer for while for the other two cases, the profile at none of the stations obey the log law. This indicates that in spite of

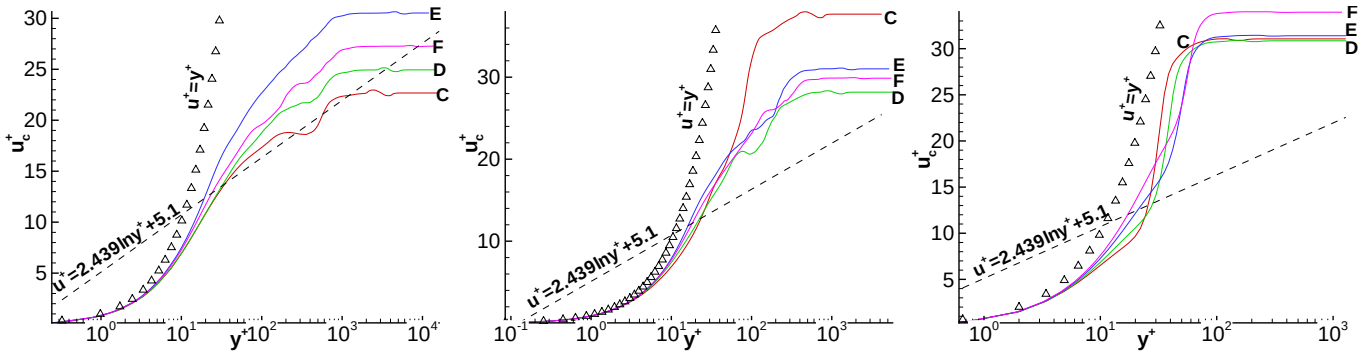

Figure 6. Van Driest transformed velocity at different locations downstream of the bump in the symmetry plate for for Ma=3.37(left), Ma=5.26(center) and Ma=8.23(right).

the flow transitioning to turbulence downstream of the bump for Ma=3.37, it does not behave like a fully developed turbulent boundary layer. For the Ma=8.23 case, the Van Driest profile confirms that the flow continues to remain laminar downstream of the bump.

IV.C. Flowfield downstream of the roughness element

We compare the flowfield downstream of the bump for the three cases considered. The spanwise variation of the instantaneous streamwise velocity in a plane very close to the flat plate at different streamwise stations downstream of the bump is shown in Fig. 7. The location downstream of the bump at which the stations are located are as specified in Section III. The horseshoe vortex which forms around the roughness element close to the flat plate can be observed for all three cases by the presence of two peaks and a valley in the streamwise wake profile at station A. For Ma=3.37, we see that multiple peaks are observed with increasing distance from the bump suggesting the transition of the flow to turbulence where the unsteady structures formed downstream appear to breakdown into even smaller structures. This observation is consistent with those made from the vorticity magnitude contours and C_f variation. Similar behavior is observed for Ma=5.26 although it is difficult to tell from the wake profile whether the flow is transitional or turbulent in nature. For Ma=8.23, we observe that the peaks formed due to the horseshoe vortex do not breakdown into multiple peaks indicating that the flow does not transition for these flow conditions. With increasing downstream distance from the bump, ultimately a flat profile is obtained. This is again consistent with the observations from vorticity magnitude contour and C_f variation, and instantaneous streamwise velocity and density contours is shown in Fig. 8.

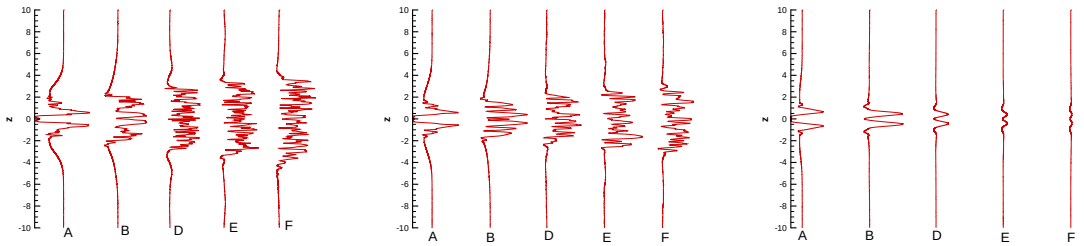

Figure 7. Evolution of instantaneous streamwise velocity profile plotted against spanwise distance for Ma=3.37(left), Ma=5.26(center) and Ma=8.23(right).

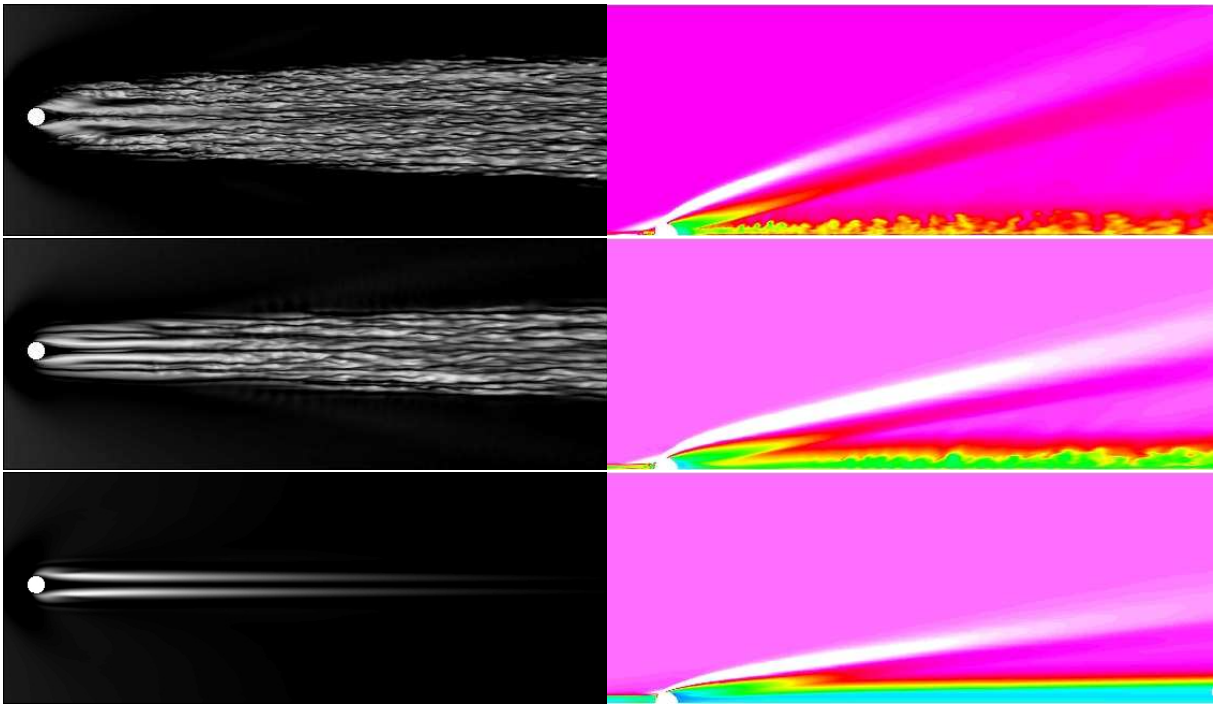

Figure 8. Instantaneous velocity contours at a wall normal plane close to the flat plate(left) and instantaneous density contours at symmetry plane(right) for Ma=3.37(top), Ma=5.26(center) and Ma=8.23(bottom).

IV.D. The effect of distributed roughness

Direct numerical simulations were performed, of supersonic flow past a flat plate with a distributed roughness patch over a part of the domain. A schematic of the roughness is shown in Fig. 9. The streamwise and spanwise directions are x and z respectively. The domain extends from x=4.0 to x=9.0 (inches). The wall–normal and spanwise extents of the domain are 0.5 and 0.175 respectively. The incoming flow is specified according to the similarity solution for a Mach 2.9 laminar boundary layer over a flat plate, with the origin at x=0. The wall is perturbed over a region $4.5 \leq x \leq 5.0$ as $y_{wall} = hsin(k_1 x)sin(k_2 z)$. As Fig. 9 shows, the roughness spans two wavelengths in the span and five wavelengths in the streamwise direction. The unit Reynolds number is 635000 (/per inch). Isothermal boundary conditions are applied at the wall, with the wall temperature set to equal the adiabatic temperature at Mach 2.9. Sutherland's formula is used to compute the molecular viscosity. The computational mesh consists of roughly 36 million hexahedral elements - 2000 in x direction, 96 in y and 192 in z. The mesh spacing is uniform in the streamwise and spanwise directions and clustered in the wall–normal direction such that the elements closest to the wall have the smallest Δy. The mesh sizes are : $\Delta x = 2.5 \times 10^{-3}$, $\Delta z = 91 \times 10^{-4}$, and $\Delta y_{min} = 5 \times 10^{-5}$.

Figure 10 presents the spatial evolution of the flow. Contours of vorticity magnitude are shown very close to the wall and at a few end planes, in the vicinity of the roughness elements. The incoming boundary layer is laminar and two–dimensional. Wall roughness perturbs the boundary layer and introduces spanwise fluctuations. The amplitude of these fluctuations increases with the downstream distance, and the flow becomes three–dimensional and turbulent. Streamwise vortices produced by the roughness elements appear coherent for some distance downstream before breaking down. Figure 11 shows snapshots at planes parallel to, and at different distances from, the wall using contours of streamwise velocity u. The first station (y = 0.005) is below the peak roughness height as can be seen. The other planes are y = 0.01, 0.015, 0.02 and 0.025. The streamwise vortices are less prominent moving farther from the wall. Figure 11 spans a larger streamwise distance than Fig. 10 and the flow appears very turbulent by x = 7.0.

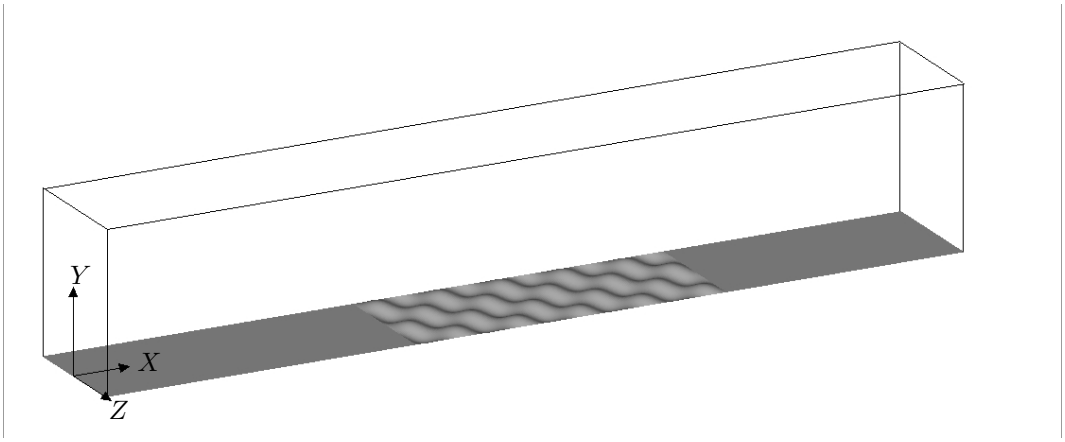

Figure 9. Schematic of the problem shows the roughness strip along with the coordinate axes. Note that the domain extends much further downstream of the roughness strip.

Figure 12 plots the variation of the skin friction coefficient(C_f) and the turbulent kinetic energy ($\overline{u_i' u_i'}$) along the length of the wall. Both these curves show that transition begins soon after $x = 5.0$ (end of the roughness patch). Peak C_f and $\overline{u_i' u_i'}$ values are observed around x =6.0 and the curves decrease thereafter as expected for developed turbulent boundary layers. Time–averaged statistics from the turbulent region of the flow are compared to available data. Figure 13 compares the Van Driest transformed velocity profiles to similar profiles from Martin *et al.*[20] and Guarini *et al.*[21] The profiles from the present simulations are from three different streamwise locations – $x = 6.5$, 7.5 and 8.5, and correspond to $Re_\theta = \rho_\infty u_\infty \theta / \mu_{wall}$ of 936, 1537 and 1849. The reported Re_θ of Guarini *et al.* is 849 and 1577 (based on μ_{wall} and μ_∞ respectively), and that of Martin *et al.* is 2390. Figure also shows comparison of the velocity profile to the experimental data of Bookey *et al.*[22] and Ekoto *et al.*[23] While the momentum thickness Reynolds number of the Bookey data is 2400, that of Ekoto *et al.* is close to 60 000. Figure 14 shows the variation of streamwise velocity u with y/δ at the three locations, and compared to similar data of Bookey *et al.*[22] and Zheltovodov *et al.*[19] The agreement appears reasonable, showing that the incoming laminar boundary layer transitions to a fully developed turbulent flow due to the surface roughness.

Case	Mach number	Roughness amplitude	Wall temperature	Reynolds number	Transitional behavior	Re_k
1	2.25	0.0025	1.9075	635000	laminar	1587.5
2	2.25	0.005	1.9075	635000	turbulent	3175
3	2.9	0.005	1.9075	635000	turbulent	3175
4	2.9	0.005	2.682	635000	laminar	3175
5	2.9	0.0075	2.682	635000	turbulent	4762.5
6	2.9	0.005	2.682	1143000	turbulent	5715

Table 2. Transitional behavior of various simulations of flow past distributed roughness. Whether the flow transitions is sensitive to all the parameters listed.

The above results correspond to simulations at Mach 2.9 with the roughness height $k = 0.0075$, and Re = 635000/inch. Simulations were also performed at different parameters, listed in table 2 to study whether the flow transition appears to be sensitive to Mach number, Re, surface roughness and the wall temperature. For example, simulations showed that flow at the same conditions, but with the roughness amplitude $k =$ 0.005 did not transition. Flow in the vicinity of the roughness, as well as downstream remained laminar.

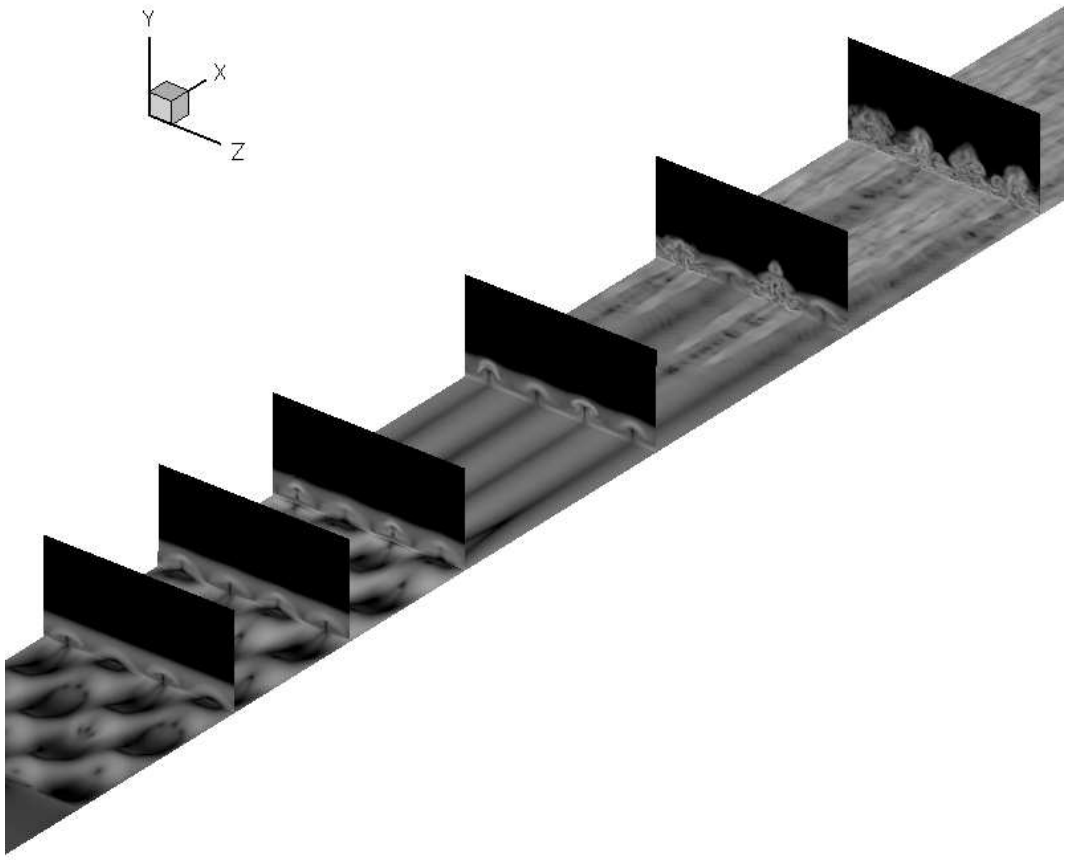

Figure 10. Snapshot of the flow showing the region near the roughness strip and the transition of the flow. Figure shows contours of magnitude of vorticity.

Figure 15 shows a snapshot from this simulation using contours of velocity u on a horizontal plane ($y = 0.01$). Note that the roughness extends between $x = 4.5$ and 5.0, and also that while the roughness produces streamwise vortices, they remain laminar throughout the length of the domain. This tendency to transition is well correlated with the local Reynolds number, $Re_{k,wall} = \rho_{wall} k u_\infty / \mu_{wall}$ and is discussed below.

IV.E. Local Reynolds number and transition

From the above discussions, the flow downstream of the hemispherical roughness element appears to transition to turbulence for Ma=3.37, become transitional for Ma=5.26 and remain laminar for Ma=8.23 case. As suggested earlier, a combination of factors could be responsible for this behavior at different flow conditions. Table 1 lists the freestream Reynolds number for the three cases considered. It is known from stability theory that compressibility stabilizes the flow and our results are consistent with this with the least Mach number flow being most unstable and therefore transitioning to turbulence. It is also known that a higher boundary layer thickness moves the transition point away from the roughness element and our results are consistent with this behavior with the lowest boundary layer thickness case (Ma=3.37) transitioning closest to the bump. The freestream Reynolds number based on roughness diameter (Re_k) is highest for Ma=8.23 which remains laminar. To account for the effect of boundary layer thickness and wall temperature, we

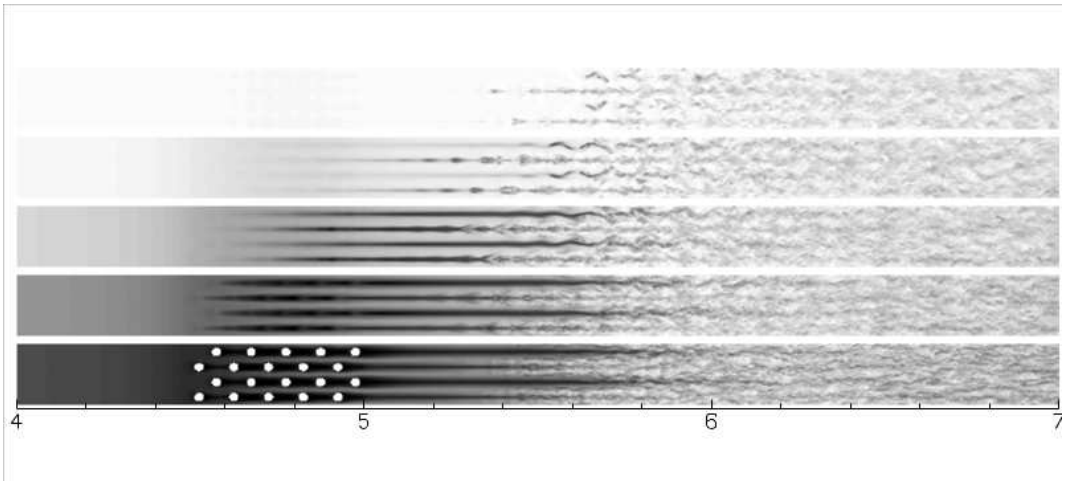

Figure 11. Snapshot of the flow using contours of streamwise velocity u. Planes parallel to the wall at $y = 0.005$, 0.01, 0.015, 0.02 and 0.025 are shown.

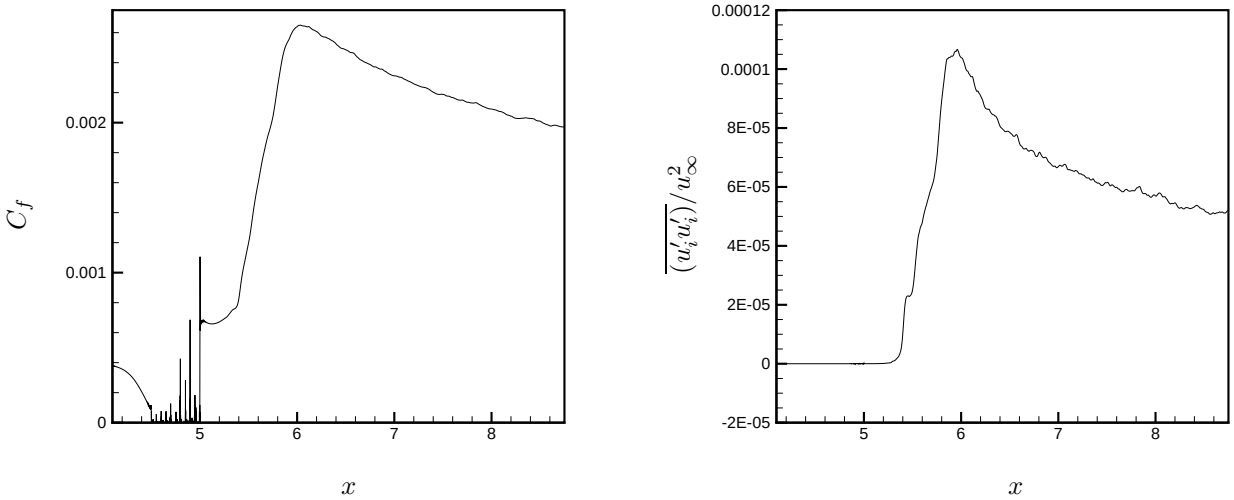

Figure 12. Variation of skin friction coefficient and turbulent kinetic energy along the wall. Note that the flow begins to transition past the roughness strip.

compute a local Reynolds number based on freestream velocity, wall kinematic viscosity and diameter of roughness ($Re_{k,wall}$) and we see that this parameter is indicative of the trend observed for transition for the three cases. Ma=8.23 has the least $Re_{k,wall}$ while Ma=3.37 has the highest $Re_{k,wall}$.

For the flow past distributed roughness, Cases 2 and 3 become turbulent whereas Case 1 remains laminar. This can be accounted for by the increase in both Re_k and $Re_{k,wall}$. With increased wall temperature compared to Case 3, Case 4 remains laminar in spite of having the same Re_k. $Re_{k,wall}$ is however much lower for Case 4 than Case 3 thus indicating that the flow may not transition. The effect of wall condition is also accounted for in this parameter and thus appears to model the trend of transition for compressible flows better than Re_k computed based on freestream parameters. Thus, from Table 3, it can be seen that the local Reynolds number correlates transition well for both isolated and distributed roughness cases.

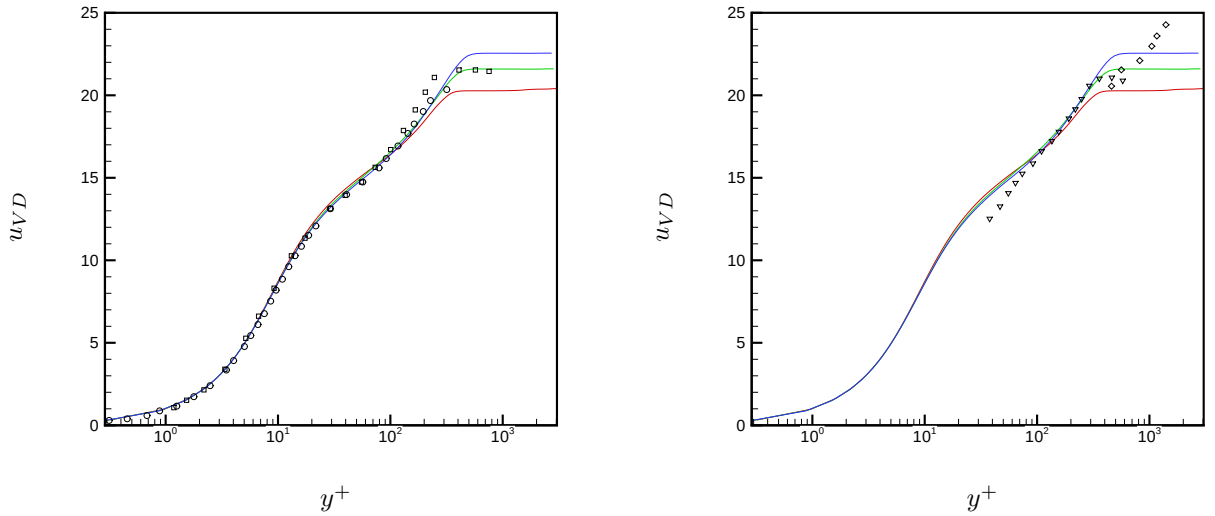

Figure 13. Comparison of Van Driest transformed velocity profiles with available data. Profiles at three streamwise locations from the simulation are compared with simulations (○ Guarini *et al.*, □ Martin *et al.*) and experiments (▽ Bookey & Smits, ◇ Ekoto *et al.*)

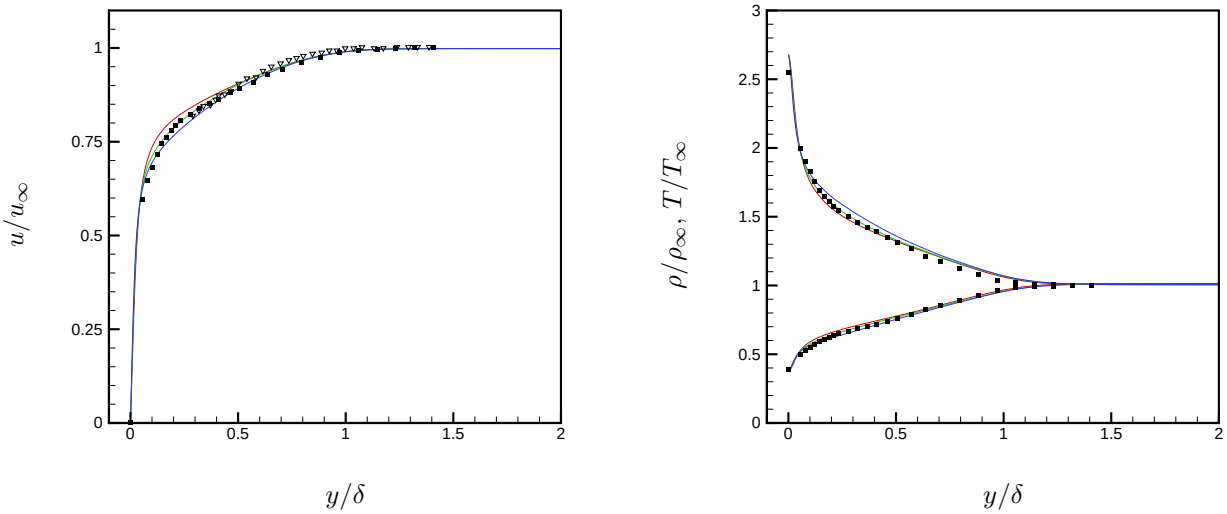

Figure 14. Comparison of simulation results with experiments. Lines show profiles from the simulation, symbols show experimental data (▽ Bookey & Smits, ■ Zheltovodov *et al.*)

V. Summary

Dierct Numerical Simulations were used to study high-speed transition induced by (I) an isolated hemispherical bump on Mach 3.37, 5.26 and 8.23 boundary layer and (II) distributed roughness on a Mach 2.9 boundary layer. The single bump simulations were performed at conditions that match those in Danehy *et al.*[1] Good qualitative agreement was found between experiment and computation. Quantitative comparison of the skin friction coefficient variation and Van Driest transformed velocity was made with the theoretical

Figure 15. Snapshot of the flow from a simulation where the flow did not transition. Mach number is 2.9, Re = 635000/inch, roughness amplitude $k = 0.005$.

Roughness type	Re_k	$\mathrm{Re}_{k,wall}$	Transitional behavior
Single	18241	22728	turbulent
	28379	9257	transitional
	33662	2208	laminar
Distributed	1587.5	480.85	laminar
	3175	961.70	turbulent
	3175	544.24	laminar
	5715	979.63	turbulent
	4762.5	816.36	turbulent

Table 3. Transitional behavior of various simulations of flow past roughness.

values for laminar and turbulent boundary layers. The flow appears to become turbulent for Ma=3.37, become transitional for Ma=5.26 and remain laminar for Ma=8.23. It was observed that the skin friction coefficient for the lowest Mach number matched the theoretical turbulent boundary layer value while the intermediate Mach number C_f value was between the theoretical laminar and turbulent values and the highest Mach number remained laminar. The Van Driest transformed velocity profile showed that the flow characteristics downstream of the bump do not agree well with those of fully developed turbulent boundary layer. The wake profiles in a wall-normal plane close to the flat plate revealed that the double peaks in the spanwise variation of instantaneous streamwise velocity formed downstream of the bump break down into smaller scales for the lower Mach numbers and just diminish in magnitude for the highest Mach number. For the flow past distributed roughness, the effect of roughness amplitude and wall temperature were studied. Higher roughness amplitude caused the flow to transition and an increased wall temperature for the same freestream Reynolds number caused the flow to remain laminar. The variation of skin friction coefficient and Turbulent Kinetic Energy along with Van Driest transformed velocity profiles confirmed transition to turbulence. Quantitative comparison of the streamwise velocity, density and temperature profiles with experiment showed good agreement indicating that the flow transitioned to a fully developed turbulent boundary layer. The Reynolds number computed based on the wall viscosity, roughness height and freestream velocity is more indicative of the onset of transition as compared to the Reynolds number computed based on freestream conditions.

Acknowledgments

This work is supported by NASA under the hypersonics NRA program and by the Air Force Office of Scientific Research under contract FA9550-04-1-0341. Computer time for the simulations was provided by the Minnesota Supercomputing Institute (MSI) and Texas Advanced Computing Center through TeraGrid

allocation. The authors would like to thank Mr. Aman Verma for help with mesh generation for the single bump.

References

[1]P. M. Danehy, Brett Bathel, Christopher Ivey, Jennifer A. Inman & Stephen B. Jones, "NO PLIF study of hypersonic transition over a discrete hemispherical roughness element,"AIAA 2009-394.

[2]P.M. Danehy, A.P. Garcia, S. Borg, A.A. Dyakonov, S.A. Berry, J.A. (Wilkes) Inman & D. W. Alderfer, "Flourescence visualization of hypersonic flow past triangular and rectangular boundary-layer trips,"AIAA-2007-0536, 45th AIAA Aerospace Sciences Meeting, Reno Nevada, January 8-11(2007).

[3]Steven P. Schneider, "Effects of Roughness on Hypersonic Boundary-Layer Transition," *Journal of Spacecraft and Rockets*, Vol 45, No. 2, March-April 2008.

[4]Saric, W. S., "Gortler Vortices," *Annual Review of Fluid Mechanics*, Vol. 26, 1994, pp. 379-409.

[5]Mack, L. M., "Boundary Layer Linear Stability Theory," *Report 709, Special Course on Stability and Transition of Laminar Flow*, AGARD, March 1984, pp. 1-81.

[6]Saric, W. S., Reed, H. L. and White, E. B., "Stability and Transition of Three-Dimensional Boundary Layers," *Annual Review of Fluid Mechanics*, Vol. 35, 2003, pp. 413-440.

[7]Reshotko, Eli., and Tumin, Anatoli., "Role of Transient Growth in Roughness-Induced Transition", *AIAA Journal*, Vol. 42, No. 4, April 2004, pp. 766-770.

[8]Reshotko, Eli., "Is Re_θ/M_e a Meaningful Transition Criterion?", *AIAA Journal*, Vol. 45, No. 7, July 2007.

[9]I. Tani, H, Komoda & Y. Komatsu, "Boundary-Layer Transition by Isolated Roughness", *Aeronautical Research Institute, University of Tokyo, Report No. 375, November 1962.*

[10]Dryden, H. L., "Review of published data on the effect of roughness on transition from laminar to turbulent flow," *J. Aeronaut. Sci. 20, 477-482(1956).*

[11]P. S. Klebanoff, W. G. Cleveland & K. D. Tidstrom, "On the evolution of a turbulent boundary layer induced by a three-dimensional roughness element", *J. Fluid Mech. (1992), vol. 237, pp. 101-187.*

[12]M. S. Acarlar & C. R. Smith, "A study of hairpin vortices in a laminar boundary layer. Part 1. Hairpin vortices generated by a hemisphere protuberance", *J. Fluid Mech (1987), vol.175, pp. 1-41.*

[13]G. R. Hall, "Interaction of the Wake from Bluff Bodies with an Initially Laminar Boundary Layer", *AIAA J., VOL. 5, NO. 8, 1967.*

[14]C. Chang & M. Choudhari, "Hypersonic Viscous Flow over Large Roughness Elements", AIAA 2009-0173

[15]J. A. Redford, N. D. Sandham & G. T. Roberts, "Roughness-induced transition of compressible laminar boundary layers", Proceedings of the Seventh IUTAM Symposium on Laminar-Turbulent Transition, Stockholm, Sweden, 2009.

[16]Park N. and Mahesh K., "Numerical and modeling issues in LES of compressible turbulent flows on unstructured grids", *AIAA* paper-722, 2007.

[17]T. Colonius., " Modeling artificial boundary conditions for compressible flow", *Annual Review of Fluid Mechanics, 36:315-345, 2004.*

[18]Schlicthting, H. T. 1979 *Boundary Layer Theory.* Mc Graw-Hill.

[19]Zheltovodov, A. A., Trofimov, V. M., Schulein, E. & Yakovlev, V. N.," An experimental documentation of supersonic turbulent flows in the vicinity of forward- and backward-facing ramps". *Tech. Rep. 2030. Institute of Theoretical and Applied Mechanics, USSR Academy of Sciences, Novosibirsk.*

[20]Martin, M. P. 2007 Direct numerical simulation of hypersonic turbulent boundary layers. Part 1. Initialization and comparison with experiments *J. FLuid Mech.* **570**

[21]Guarini, S. E, Moser, R. D, Shariff, K & Wray, A. 2000 Direct nimerical simulation of a supersonic turbulent boundary layer at Mach 2.5, *J. Fluid Mech.* **414**.

[22]Bookey, P., Wyckham, C., Smits, A. & Martin, M. P. 2005 New Experimental Data of STBLI at DNS/LES Accessible Reynolds Numbers, *AIAA Paper* 2005–309

[23]Ekoto, I. W., Bowersox, R. D. W, Beutner, T & Goss, L. 2008 Supersonic Boundary Layers with Periodic Surface Roughness *AIAA J.* **46**